



Original article

Antibacterial action of insect chitosan/gum Arabic nanocomposites encapsulating eugenol and selenium nanoparticles



Mousa Abdullah Alghuthaymi

Department of Biology, Science and Humanities College, Shaqra University, Alquwayyah, Saudi Arabia

ARTICLE INFO

Article history:

Received 5 April 2022

Revised 4 June 2022

Accepted 2 July 2022

Available online 8 July 2022

Keywords:

Biopolymers
Nanocomposites
Antimicrobial
Green synthesis
Mode of action

ABSTRACT

The nanopolymers compositing and utilization for bioactive materials delivery could provide more bio-efficacy and biosafety targeting biological systems. Chitosan (CT) was extracted from black soldier fly “BSF; *Hermetia illucens*” fly and transformed to nanoparticles (NCT) via conjugation with gum Arabic (GA). Eugenol (Eug) and biosynthesized selenium nanoparticles (SeNPs) were innovatively loaded into NCT/GA nanocomposite and the entire composites were characterized and evaluated as antibacterial agents. The fabricated nanocomposites (SeNPs, NCT/GA, NCT/GA/Eug and NCT/GA/Eug/SeNPs) had mean particles sized of 9.7, 124.8, 132.6 and 134.2 nm, respectively, and the entire polymers nanocomposites carried positive charges of $>+30$ mV. The bacterial killing actions of fabricated polymers nanocomposites (NCT/GA) and their conjugates with Eug and SeNPs were assessed qualitatively and quantitatively and confirmed through scanning microscope imaging against Gram+ (*Escherichia coli*) and Gram- (*Staphylococcus aureus*) bacteria. Results indicated the forceful action of NCT/GA/Eug/SeNPs nanocomposites toward both strains, which significantly exceeded the standard antibiotic. The treated bacteria with NCT/GA/Eug/SeNPs had vigorous deformations and distortions in structures after 5 h and were completely lysed/exploded after 10 h of exposure. The outcomes could recommend the applications of innovatively synthesized NCT/GA/Eug/SeNPs as powerful antimicrobial nanocomposite for potential usage in food and pharmaceutical sectors.

© 2022 The Author(s). Published by Elsevier B.V. on behalf of King Saud University. This is an open access article under the CC BY license (<http://creativecommons.org/licenses/by/4.0/>).

1. Introduction

Chitosan (CT) is the deacetylated biopolymeric aminopolysaccharide that derived from chitin; CT as a superior biomolecule has plentiful applications in biomedical, environmental, nutritional and biological fields, with diverse sources for its production (including crustacean shells, plants, fungi, and insects) (Kou et al., 2021). The CT bioactivities were frequently confirmed, as talented antimicrobial, antioxidant, clarifying, healing accelerator, biochelating, and fungicidal agent (Tayel et al., 2010; Marei et al., 2019; Ke et al., 2021). Although marine crustacean wastes are the prime CT extraction sources, due to unregulated production, seasonal variations and inadequate supply, fungi and insects are explored as hopeful alternatives for CT extraction (Luo et al.,

2019). The number of insect species is estimated to reach 10 million, which exceeds the entire other animals' types together (Hahn et al., 2020). Numerous investigations succeeded to extract CT from divers insect species, including *Calosoma rugosa*, *Apis mellifera*, *Schistocerca gregaria*, and Black soldier fly “BSF, *Hermetia illucens*” (Marei et al., 2016; 2019; Mertenat et al., 2019; Luo et al., 2019). BSF is the fly that can be farmed for having alternative rich sources of protein for feeding poultry, animals, and fish; the BSF exoskeleton have significant amounts of chitin, which could be utilizable for CT extraction (Mertenat et al., 2019; Al-saggaf, 2021).

The applications of nanomaterials/nanotechnology in daily life became a real fact; they are currently involved in most human activities such as nutritional, agricultural, industrial, biomedical and pharmaceutical fields (Kolahalam et al., 2019). These extensive applications of nanoparticles (NPs) enforced the researches for further effectual, economical and ecofriendly methods to generate and manipulate such nano-forms (Pandit et al., 2022). The conventional NPs synthesizing procedures (chemically and physically) had numerous limitations for metals NPs preparation, e.g. elevated-energy requirements, toxic /hazardous chemical residues,

Peer review under responsibility of King Saud University.



Production and hosting by Elsevier

<https://doi.org/10.1016/j.jksus.2022.102219>1018-3647/© 2022 The Author(s). Published by Elsevier B.V. on behalf of King Saud University. This is an open access article under the CC BY license (<http://creativecommons.org/licenses/by/4.0/>).

complicated instruments, and downstream practices' cost (Kolahalalam et al., 2019; Pandit et al., 2022).

The NPs "Green synthesis" strategies are involving the utilization of biological sources (bacteria, plants, biopolymers, fungi ...etc) or their derivatives/constituents for NPs synthesizing (Pandit et al., 2022). The biosynthesis approaches provide numerous advantages over traditional methods, e.g. cost-effectiveness, vast production, high yield, more safe NPs products, and eco-friendly processes (Kolahalalam et al., 2019; Begum et al., 2021).

Eugenol (Eug) is the natural phenolic compound (volatile terpene) that forms the principal percentages in multiple essential plant oils, e.g. *Syzygium aromaticum*, *Cinnamomum verum*, *Piper betle*, and *Myristica fragrans* (Anand et al., 2021). Eug recurrently exhibited potent bioactivities, which enable its application as a potent antibacterial, antioxidant, anti-inflammatory, preservative, antifungal and antitermitic agent (Marchese et al., 2017; Bonilla et al., 2018; Yassin et al., 2020). Eug also was recognized as non-carcinogenic, non-mutagenic and as generally safe compound (GRAS) for application in human food (Wang et al., 2020; Yassin et al., 2020). Despite the numerous bioactivities of Eug, its biomedical and nutritional applicability is seriously limited because of its poor water solubility, speedy metabolism/excretion, instability, and high sensitivity to oxidation, heat and light (Bonilla et al., 2018; Wang et al., 2020; Oluoch et al., 2021).

Nano-encapsulation and nano-conjugation of bioactive molecules within biopolymers (e.g. chitosan) NPs can provide many beneficial advantages to boost their physical stability, bioactivity and deliverability to target tissues/organs (Argüelles-Monal et al., 2018). Such techniques could also reduce potential toxicity of bioactive compounds, their sensitivity to heat/light and prevent interactions of active agents with food constituents (Anand et al., 2021).

The Se element (Selenium) is extremely essential for biological bodies (as the chief constituents in selenoproteins, prooxidative and antioxidative agent), with daily requirement of 30–300 µg and µg/day for human body, which give Se elevated significance in medicine and nutrition (Hosnedlova et al., 2017; Zaynab et al., 2022). Se performs prime roles in cellular metabolism, enzymes' activation, free radical protection, thyroid metabolism, human fertility, and other numerous bio-functionalities; this promoted its involvement in miscellaneous biomedical fields as antitumor, antioxidant, enzyme regulator, cytokine inducer, anti-infective, and immunomodulator agent (Hosnedlova et al., 2017; Kumar and Prasad, 2021). The nanoparticles of Se (SeNPs) have could be effectually synthesized via diverse protocols, with preference to biosynthesizing approaches, which provide SeNPs with surplus bioactivities and much lower-toxicity than bulk Se for usages in nutritional, antimicrobial and anticancer applications (Zhang et al., 2001; Kumar and Prasad, 2021).

The coating, conjugation and stabilization of such metals' NPs with biopolymers (e.g. chitosan, gums, gelatin, alginate, ...etc) and their NPs provide them more applicability, deliverability, bioactivity and biosafety for direct employment in biomedical, pharmaceutical, environmental and food-related applications (Tan et al., 2016; Alghuthaymi et al., 2021; Siddiqui and Alrumman, 2021).

Accordingly, current study targeted the extraction of CT from BSF and transforming it to NPs and to conjugate it with Eug/SeNPs, to provide potential potent antibacterial nanocomposites for controlling bacterial pathogens.

2. Materials and method

2.1. Materials

Spray-dried Acacia gum (Gum Arabic; GA, Merck Millipore, Germany); eugenol (Eug), acetic acid, Tween 80, hydrochloric acid

(HCl, 37%), sodium selenite ($\text{Na}_2\text{SeO}_3 \cdot 5\text{H}_2\text{O}$), ethanol ($\geq 99.8\%$), triphenyl tetrazolium chloride (TTC), L-ascorbic acid (99%), methanol (99.9%, HPLC-grade), chloroform (HPLC-grade, 99.5+%), sodium hydroxide (NaOH, anhydrous, $\geq 98\%$), and microbiological media (obtained from Sigma-Aldrich, MO), were used throughout current study.

2.2. Insect chitosan extraction

Insect CT was extracted from BSF "*Hermetia illucens* larvae", which were attained from the "Experimental insect farm, University of King Abdulaziz, Jeddah, KSA", at their 5th instar. The insects' proteins and oils were mostly eliminated via oil-press approach, and BSF residues were rinsed with double-distilled water (DW), and then lyophilized. The CT extraction from BSF residual materials involved (Marei et al., 2016; Al-saggaf, 2021):

- 1- Defatting: by treatment with 12 folds (v/w) of chloroform-methanol mix (7:3, respectively) under stirring for 5 h at room temperature (RT; $25 \pm 2^\circ\text{C}$).
- 2- Demineralization: by treatment of resulted materials from (1) with 12 folds (v/w) of 2% HCl solution for 2 h at RT.
- 3- Deproteinization: by treatment of resulted materials from (2) with 10 folds (v/w) of 1.0 M NaOH solution at $48 \pm 2^\circ\text{C}$ for 3 h.
- 4- Deacetylation: by treatment of resulted materials from (3) with 20 folds (v/w) of concentrated NaOH (58%, w/v) solution, at RT for 1 h then at 115°C for 2 h. The extensive DW washing and air drying was performed after every step, and the final resulted CT was then lyophilized. For the lyophilization of CT and subsequent composites, the vials of lab-scale benchtop lyophilizer (VirTis adVantage Plus; SP Scientific, Gardiner, NY) were filled with composites' solution, stoppered and positioned into the instrument tray. The lyophilization was performed at -40°C for 22 h with 0.111 kPa chamber pressure.

2.3. Preparation of biopolymers nanocomposites

For preparing polymers nanocomposite from inset NCT, GA, Eug and SeNPs, the GA and extracted CT were firstly dissolved (at 0.1%, w/v) in DW and acetic acid 0.1%, respectively. The pH of dissolute CT solution was modified to 4.8 by adding few drops (when necessary) from 0.2 M NaOH solution, and then Eug and Tween 80 were added to this solution (at 0.1%, v/v each) while stirring at 520g at RT. After that, GA solution was dropped slowly into this solution while stirred. The stirring continued for further 2 h, and then the mixing solution was centrifuged at 11500g for 22 min (Sigma 2-16P-10350, GmbH, Germany). The supernatant was collected, recurrently washed with DW, re-centrifuged and lyophilized (Rajabi et al., 2019).

For NCT/GA/Eug/SeNPs nano-compositing, 100 µM of sodium selenite was dissolved in GA solution before dropping and the chitosan/Eug solution was supplemented with 0.1% (w/v) of ascorbic acid, as precursor for SeNPs reduction, and the step were conducted as above. The formed nanocomposites were purified via repeated washing by DW and ethanol, followed by centrifugation after each wash and pellets' harvesting, to eliminate the excess free molecules.

2.4. Analysis of materials physiognomies

2.4.1. FTIR "Fourier-Transform Infrared Spectroscopy" analysis

The FTIR (Perkin Elmer, Germany) was employed for analyzing the Infrared spectroscopic patterns of NCT, GA, NCT/GA and NCT/GA/Eug composites. The screened materials/composites analysis

was performed in the FTIR transmission mode, following their amalgamation with 1% KBr, at 400–4000 cm^{-1} wavenumber range.

2.4.2. Structural analysis

The TEM “Leo 0430 Transmission electron microscopy, Leica, UK” was used for imaging the organizational features “morphology, shape, distribution and size” of biosynthesized SeNPs.

2.4.3. The assessment of zeta potential and particles' size (Ps)

The assessments of particles charges (zeta potential) and Ps distribution of fabricated nanocomposites, e.g. NCT/GA, NCT/GA/Eug and NCT/GA/Eug/SeNPs, were performed using Malvern Zetasizer “Nano ZS instrument, MA”.

2.5. The encapsulation efficiency (EE) and loading capacity (LC) of Eug-loaded nanopolymers

The EE and LC of Eug encapsulated into NCT/GA nanocomposite were analyzed according to [Woranuch and Yoksan \(2013\)](#). The dispersed sample in DW was combined with 5% (v/v) of 1 M HCl and heated to 96 °C for 32 min. Ethanol (1%, v/v) was introduced to the mixture, then it was centrifuged at 7500g for 1 min at RT. The gathered supernatant absorbance was measured via UV–vis spectrophotometry at 283.5 nm wavelength. The EE and LC of Eug in nanopolymers were calculated as follow:

$$EE(\%) = [\text{weight of loaded Eug}/\text{weight of initial Eug}] \times 100$$

$$LC(\%) = [\text{weight of loaded Eug}/\text{weight of sample}] \times 100$$

2.6. Antibacterial assessment of nanopolymers-based composites

The antibacterial assessment of NCT/GA, NCT/GA/Eug and NCT/GA/Eug/SeNPs involved diverse techniques for qualitative, quantitative and imaging examination.

2.6.1. Bacteria cultures

Standard bacterial strains “i.e. *Escherichia coli* ATCC-25922 and *Staphylococcus aureus* ATCC-25923” were employed as models for Gram-negative and Gram-positive bacteria, respectively. Bacteria were propagated and challenged using NB and NA “nutrient broth and Nutrient agar media, respectively”, aerobically at 37 ± 1 °C.

2.6.2. Qualitative antimicrobial examination of nanocomposites

The ZOI assay “zones of bacterial inhibition”, by disc diffusion technique, was applied after exposure of bacteria to nanocomposites ([Tayel et al., 2010](#)). Sterile discs (6 mm diameter) of Whatman No. 2 filter paper were loaded (25 $\mu\text{L}/\text{disc}$) with 2% aqueous solutions from of NCT/GA, NCT/GA/Eug and NCT/GA/Eug/SeNPs and positioned on the surfaces of freshly inoculated NA plates with bacterial cultures. After incubation at 37 °C for 20–24 h, the witnessed ZOI diameters were measured accurately in triplicates and their means were reckoned. Ampicillin (CAS no. “69-52-3”, Sigma-Aldrich, MO) was acted as the positive antibacterial control, whereas acidified DW (pH 4.8) was the negative control for comparison.

2.6.3. Quantitative antimicrobial examination of nanocomposites

The MIC “minimal inhibitory concentrations” of NCT/GA, NCT/GA/Eug and NCT/GA/Eug/SeNPs were valued via microdilution ([Tayel et al., 2012](#)). Bacterial cultures were inoculated in 96-wells microplates having NB medium to reach $\sim 2 \times 10^7$ cell/mL, and then serial concentrations from biopolymers nanocomposites (at 5–100 $\mu\text{g}/\text{mL}$ range) were added to wells and the plates were incubated for 16–18 h at 37 °C. TTC indicator was added to suspected wells to confirm bactericidal action of nanocomposites.

2.6.4. SEM “Scanning microscopy” imaging

The SEM “Scanning electron microscopy, JSM IT200; JEOL, Japan” was used for detecting the morphological alterations in treated bacterial cells with NCT/GA/Eug/SeNPs for 0, 5 and 10 h of treatment and incubation at 37 °C. Cells were exposed to $2 \times$ MICs of the nanocomposite, and the image capturing tracked the structural distortions in exposed cells.

2.7. Statistical analysis

Experiments in triplicates were performed, the SPSS package (V 11.5, Chicago, USA) was used for computing means \pm SD (standard deviation) and the differences' significances at $p \leq 0.05$ were computed using one-way ANOVA and *t*-test.

3. Results and discussion

3.1. Chitosan extraction from BSF

The CT was efficaciously extracted from larval biomass of BSF; the yielded purified CT reached 1.62%, with 88.2% deacetylation degree, molecular weight of 95.7 kDa and solubility of 97.1% in diluted acetic acid (1%, v/v). The attained physiochemical characteristics of BSF-CT here are comparable to the formerly obtained from recent investigations ([Marei et al., 2016](#); [Al-saggaf, 2021](#)).

3.2. Infra-red analysis of produced molecules

The biochemical bonding and interactions of employed molecules (NCT, GA, Eug and their composites) were analyzed spectroscopically via FTIR ([Fig. 1](#)).

For NCT ([Fig. 1-NCT](#)), the spectral analysis indicated the occurrence of most distinctive bonding in extracted CT from insects, which were illustrated in earlier investigations ([Marei et al., 2016](#); [Luo et al., 2019](#); [Hahn et al., 2020](#)). The main distinctive bands in NCT were positioned at 3414 cm^{-1} (pertained to overlapped O–H and N–H extensional vibrations), 1568 cm^{-1} (N–H bending vibration), 1415 cm^{-1} (C–H extensional vibration) Additionally, the following characteristic bands were appeared an derived from native CT, at 2913 cm^{-1} (C–H stretching), 1642 cm^{-1} (amide I), 1538 cm^{-1} (amide II), 1079 cm^{-1} (C–O–C), and at 904 cm^{-1} (pyranose ring) ([Luo et al., 2019](#); [Hahn et al., 2020](#); [Al-saggaf, 2021](#)). The specified peak for CT-TPP binding and forming of P=O linkage was detected at 1251 cm^{-1} , confirming NCT formation ([Anand et al., 2021](#)).

The GA spectrum ([Fig. 1-GA](#)) displayed the distinguishing band for this biopolymer; including the sharp bands at 1622 and 1413 cm^{-1} (assigning the asymmetrical and symmetrical vibrations of carboxyl groups, respectively), at 2911 cm^{-1} (C–H extension), and around 3400 cm^{-1} (O–H extensional vibrations) ([Espinosa-Andrews et al., 2010](#); [Tan et al., 2016](#); [Rajabi et al., 2019](#)).

The band at 2911 cm^{-1} could signify the existence of sugars, e.g. arabinose, galactose, and rhamnose. The 1622 cm^{-1} band indicates occurrence of amino acids and aromatic/aliphatic galactoproteins, along with the 1376 cm^{-1} band. The glucuronic acids indicative band (at 1413 cm^{-1}) is attributed to symmetric C=O stretching. Additionally, the 1252 cm^{-1} band could represent C–O alcohol stretch, alkane CH_3 , stretching ether C–O–C or stretching amines C–N, whereas the 1024 cm^{-1} band represents bending alkene C–H from gum polysaccharides ([Rajabi et al., 2019](#)).

The conjugated NCT/GA nanoparticles spectrum ([Fig. 1-NCT/GA](#)) has many distinctive peaks from both biopolymers, and shifting of other specified peaks after conjugations (e.g. the band at 1622 cm^{-1} in GA spectrum shifted to 1578 cm^{-1} in NCT/GA spec-

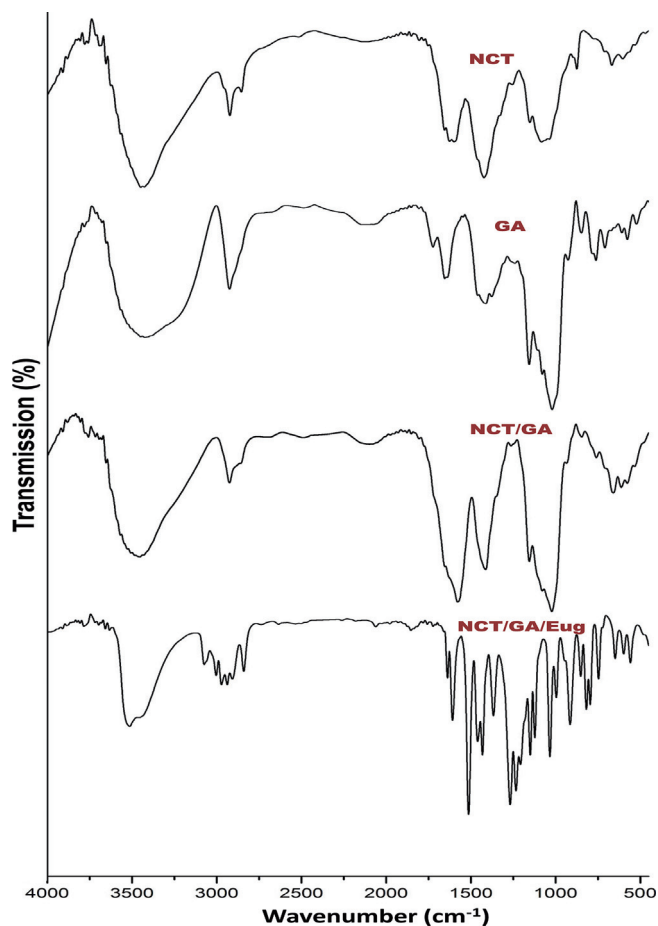


Fig. 1. FTIR spectra of fabricated biomolecules/composites, including insect chitosan nanoparticles (NCT), gum Arabic (GA) and eugenol (Eug).

trum), which indicate physical/chemical interactions after polymers' conjugation (Avadi et al., 2010; Espinosa-Andrews et al., 2010; Rajabi et al., 2019).

The FTIR spectrum of loaded Eug into NCT/GA nanocomposite reflected the main distinctive peaks of Eug in addition to the biopolymers characteristic peaks (Fig. 1-NCT/GA/Eug). The Eug distinctive bands were clearly detected at 3077 and 2999 cm^{-1} (=C–H vibrated stretching), at 1508 and 1607 cm^{-1} (C=C vibrated stretching in aromatic rings), at 1261 and 1203 cm^{-1} (C–O bending vibration), at 891 cm^{-1} (–C=CH₂ bending), at 741 cm^{-1} (–CH₂ bending), and at 1358 cm^{-1} (–CH₃ bending) (Woranuch and Yoksan, 2013; Anand et al., 2021; Das et al., 2021). the detection of bands at

Table 1

Size and charge of biopolymers nanocomposites \pm SD (standard deviation).

Nanoparticles	Mean diameter (nm)	Size range (nm)	Zeta potential (mV)
NCT/GA	124.8 \pm 19.6	71.4–282.1	+38.7 \pm 6.3
NCT/GA/Eug	132.6 \pm 21.7	76.5–308.2	+35.4 \pm 5.1
NCT/GA/Eug/SeNPs	134.2 \pm 33.5	77.6–337.5	+31.8 \pm 4.9

1231 and 1120 cm^{-1} that appointed ionic-crosslink formation between TPP and NH³⁺ groups in NCT, in addition to Eug distinctive bands in NCT/GA/Eug composite, strongly validated the physico-chemical conjugation between the composite materials of chitosan and anionic groups conjugation (Bonilla et al., 2018; Anand et al., 2021; Das et al., 2021).

3.3. Structural analysis of fabricated nanoparticles/nanocomposites

The structural physiognomies of fabricated nanocomposites are demonstrated in Table 1 and Fig. 2. The NCT/GA nanocomposite have homogenous and well-dispersed characteristics, with mean Ps diameter of 124.8 nm, whereas the NCT/GA/Eug composite were had slightly larger Ps mean diameter (132.6 nm) and this mean additionally increased (134.2 nm) with the incorporation of SeNPs to form NCT/GA/Eug/SeNPs composite. The entire nanocomposites (NCT/GA, NCT/GA/Eug, and NCT/GA/Eug/SeNPs) carried strong positive charges on their surface (e.g. zeta potential > 30 mV); the highest positivity was recorded for NCT/GA (+38.7 mV) and slightly reduced with the incorporation of further molecules to nanocomposites. The used ratio and pH for NCT/GA composite fabrication were should be 1:1 (w/w) and 4.0, respectively, which was formerly illustrated as the optimal conditions for this nanocomposite construction (Tan et al., 2016); the resulted nanoparticles with this technique/condition have high affinity for encapsulating hydrophobic molecules. The illustrated mechanism for producing NCT/GA nanocomposites, which are highly stable, is the interaction between positively charged amine groups in NCT with negative charges in GA surface; the excess positive charges in NCT groups give the composite its positive values of zeta potential (Avadi et al., 2010; Pant and Negi, 2018).

The slight increase in Ps of NCT/GA/Eug and NCT/GA/Eug/SeNPs composites than the Ps of plain NCT/GA, and the decrease of the nanocomposites' zeta potential after incorporation of Eug and SeNPs, both indicate that NCT/GA could entrap/uphold the other molecules within their matrix. This feature generally leads to Ps enlargement and occupation of some free charges with these added molecules, which cause zeta potential reductions (Tan et al., 2016; Rajabi et al., 2019).

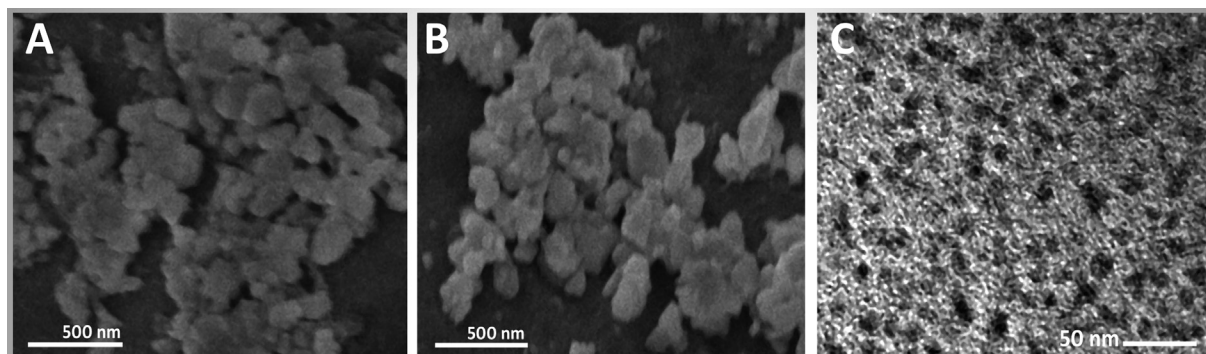


Fig. 2. Electron microscopy imaging of produced nanomaterials including the SEM of insect chitosan/gum Arabic nanocomposite (A), their loaded particles with eugenol (B), and the TEM imaging of eugenol-mediated SeNPs (C).

Table 2
Antibacterial potentialities of generated polymers nanocomposites and their conjugates with eugenol and SeNPs.

Nanocomposite	Antibacterial potentials*					
	<i>Escherichia coli</i>			<i>Staphylococcus aureus</i>		
	ZOI** (mm)	MIC ($\mu\text{g}/\text{mL}$)	MBC ($\mu\text{g}/\text{mL}$)	ZOI (mm)	MIC ($\mu\text{g}/\text{mL}$)	MBC ($\mu\text{g}/\text{mL}$)
NCT/GA	10.5 \pm 1.4 ^a	35.0	37.5	11.1 \pm 1.8 ^a	40.0	45.0
NCT/GA/Eug	18.3 \pm 2.2 ^b	25.0	27.5	17.1 \pm 2.1 ^b	27.5	32.5
NCT/GA/Eug/SeNPs	22.4 \pm 3.4 ^c	15.0	15.0	20.7 \pm 2.9 ^c	20.0	17.5
Ampicillin	18.5 \pm 2.6 ^b	27.5	27.5	16.8 \pm 2.5 ^b	30.0	32.5

* The antibacterial assays included inhibition zone measurements (ZOI, in mm) \pm SD (standard deviation), minimal inhibitory and bactericidal concentration (MIC and MBC, respectively; in 1–50 $\mu\text{g}/\text{mL}$ range).

** “Dissimilar superscript letters in one column indicate significant difference at $p \leq 0.05$ ”.

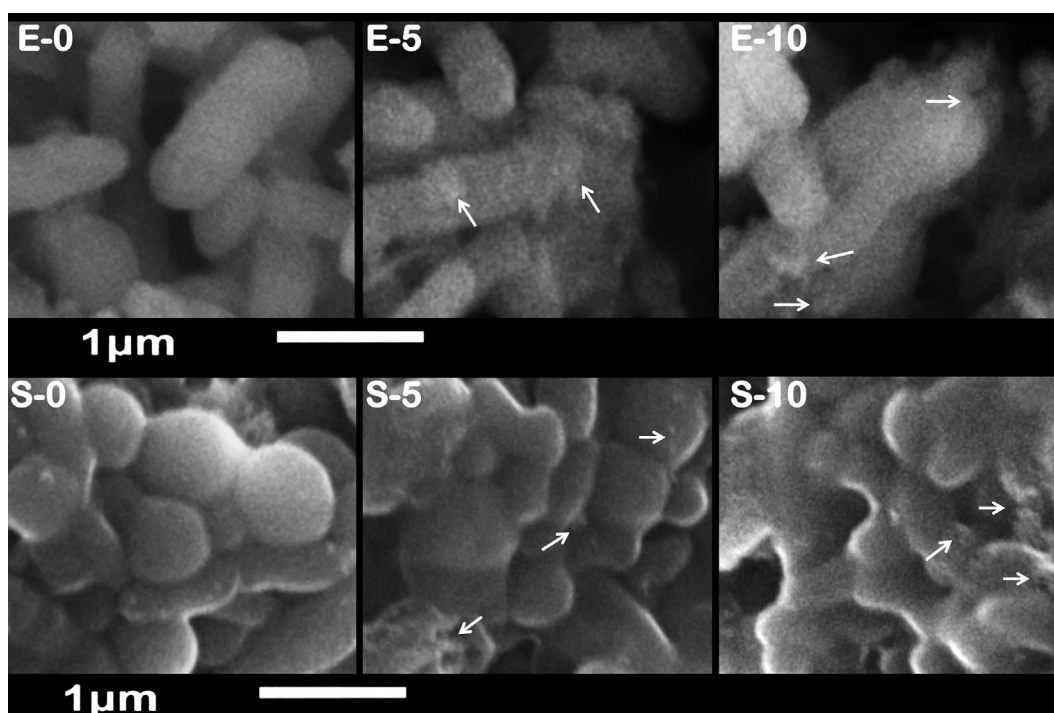


Fig. 3. Scanning imaging of exposed *Escherichia coli* (E) and *Staphylococcus aureus* (S) cells to nanocomposite of chitosan/gum Arabic/eugenol/SeNPs for 0, 5 and 10 h. Arrows indicate examples of attached nanoparticles to microbial cells.

The calculated EE and LC of NCT/GA toward Eug were $71.94 \pm 0.42\%$ and $17.45 \pm 0.34\%$, respectively. The LC represented the quantity of loaded Eug per weight unit of biopolymer matrix, while EE denoted the efficacy of biopolymers to protect the loaded Eug (Das et al., 2021); the EE is economically very important for nanocapsules' fabrication (Woranuch and Yoksan, 2013; Rajabi et al., 2019). The encapsulation into nanopolymers (e.g. NCT) was validated to augment Eug thermal stability, and the used ratios from Eug to nanopolymer were reported as the optimum to have stronger and thicker layer around bioactive molecules and gave higher EE (Woranuch and Yoksan, 2013; Rajabi et al., 2019). Additionally, the employment of Tween-80 emulsifier in Eug encapsulation in core of NCT led to elevated percentages for EE and LC (Das et al., 2021).

3.4. Antibacterial assessment

The bacterial inhibitory actions of fabricated polymers nanocomposites (NCT/GA) and their conjugates with Eug and SeNPs were assessed qualitatively (via ZOI measurement), quanti-

tatively (via MIC and MBC determination) and confirmed through SEM imaging for the Gram- (*E. coli*) and Gram⁺ (*S. aureus*) bacteria (Table 2 and Fig. 3, respectively).

3.4.1. In vitro antibacterial assays

The findings of *in vitro* assays designated the powerful actions of screened composites (NCT/GA, NCT/GA/Eug and NCT/GA/Eug/SeNPs) against challenged strains (Table 2). The entire nanocomposites displayed strong bactericidal actions; the NCT/GA/Eug/SeNPs nanoconjugate significantly exhibited the most forceful actions toward both examined bacterial strains followed by NCT/GA/Eug nanocomposite. *S. aureus* comparably possessed more sensitivity than *E. coli* toward examined nanocomposites, which was evinced from the higher ZOI diameters and lower values from MICs and MBCs. The antibacterial action of NCT/GA/Eug/SeNPs nanocomposite significantly exceeded the control antibiotic (ampicillin), in both bacterial strains.

The wide potent antimicrobial spectra (e.g. antifungal, antimycotic, and antibacterial) of *S. aromaticum* oils, and Eug as the main constituent, was recurrently proved and reviewed (Marchese et al.,

2017; Yassin et al., 2020). The antimicrobial synergism after conjugation of NCT/GA with Eug was proved to exhibit stronger actions; because the difficulty for a microbial pathogen to resist diverse actions from different antimicrobial agents (Tayel et al., 2012, 2020). These findings support recently reported results that demonstrated the synergism between phytochemicals and other bioactive molecules (e.g. nanometals and antibiotics) toward effectual control of pathogenic resistant bacteria (Ameen et al., 2022; Begum et al., 2022; Subramaniyan et al., 2022).

The augmentation of Eug antimicrobial activity, by encapsulation with nanopolymers like NCT, was proved and evidenced with significant lower MIC values (Oluoch et al., 2021). This MIC reduction was accredited to the antibacterial action persistence, resulted from sustained biomolecules' release, and the synergism between bioactive compounds and NCT (Oluoch et al., 2021). The nano-encapsulation of Eug in gelatin and chitosan sustained its release and could significantly prolong the antibacterial and antiseptic action of the nanocomposite (Wang et al., 2020). The Eug encapsulation and immobilization in polymers matrix was reported to augment its antimicrobial actions and sustain this action for prolonged time; which was employed for extending the shelf lives of many foodstuffs (Wang et al., 2020).

3.4.2. Morphological structure of treated bacteria with nanocomposite

The antibacterial action of NCT/GA/Eug/SeNPs nanocomposite was further elucidated throughout SEM imaging of exposed bacteria (*E. coli* and *S. aureus*) to the fabricated composite for different exposure period (Fig. 3). At exposure beginning (E-0 and S-0 in Fig. 3), the cells' appearance was natural, with contacted and smooth surfaces; some nanocomposite particles were detectable in attachment with bacterial outer membranes. After exposure for 5 h (E-5 and S-5), the deformations and distortions in cells were evidenced, most cells began to lose their distinctive features and their membranes entered the lysis phase. Lastly, after 10 h (E-10 and S-10), the exposed cells to nanocomposite were mostly lysed or exploded, and the bacterial action was more vigorous in *E. coli* cells, as their cells' interior components and the residues of their walls were the only observable materials in images.

The cells' destruction action of NCT/GA/Eug/SeNPs depended on the combined actions from the composite constituents. Many reports principally attributed the Eug antimicrobial actions to the interactions with microbial cells' membranes and phospholipids, denaturation of wall protein and distortion of membranes' permeability (Marchese et al., 2017; Yassin et al., 2020); the treatments of bacteria with Eug-containing extracts could cause severe distortions and deformations in cell membranes (Tayel et al., 2020). The protection of Eug from environmental stresses was reported through encapsulation into NCT and/or GA; this protocol gives Eug more interaction with bacteria surface proteins via the strong anionic actions of the composite, which can increase cellular membranes' permeability, enforce the disruption of wall integrity, and lead to general increase in Eug antimicrobial activity (Shao et al., 2018). The Eug bioactivities for affecting bacterial membranes were attributed to serial mechanisms that involve cell morphology alteration, prompting of cellular constituents leakage, and upsurge their permeability (Tayel et al., 2020). Additionally, the strong electrostatic interactions between negatively charged cell membranes/walls and positively charged NCT could increase the nanopolymer attachment to bacterial cells and its penetration and interactions with interior organelles of bacteria (Tayel et al., 2020), along with other carried biomolecules in NCT. Accordingly, the encapsulated biomolecules (e.g. Eug) into nanopolymers (e.g. NCT and GA) could have additional probabilities for distorting bacterial cell walls/membranes, and interfering with cells' energetic components and functions to prohibit them, disrupt outer membranes' synthesis and obstruct cells' development (Tayel et al., 2010).

NCT was additionally stated to have elevated affinity for attaching microbial surfaces and inducing severe walls' lyses, deformation, disruption and explosion (Tayel et al., 2010; Tayel et al., 2012; Moussa et al., 2013; Al-saggaf, 2021).

4. Conclusion

The BSF insects could be suggested as promising source for CT production, with 1.62% yield, 88.2% deacetylation degree, and 95.7 kDa molecular weight. The construction of NCT/GA nanocomposite was achieved, with 124.8 nm mean diameter, and served as effectual carriers for other bioactive molecules. Eug and biosynthesized SeNPs could effectually loaded into NCT/GA nanocomposite, with EE and LC of NCT/GA toward Eug were 71.94 ± 0.42 and $17.45 \pm 0.34\%$, respectively. The entire fabricated nanocomposite exhibited potent antibacterial activity and cells' destruction capability within 5–10 h of exposure. The attained results could recommend the applications of NCT/GA/Eug/SeNPs as powerful antimicrobial nanocomposite for usage in food and pharmaceutical sectors.

Declaration of Competing Interest

The author declares that he has no known competing financial interests or personal relationships that could have appeared to influence the work reported in this paper.

Acknowledgements

The author would like to thank the Deanship of Scientific Research at Shaqra University, KSA, for supporting this work.

Appendix A. Supplementary data

Supplementary data to this article can be found online at <https://doi.org/10.1016/j.jksus.2022.102219>.

References

- Alghuthaymi, M.A., Diab, A.M., Elzahy, A.F., Mazrou, K.E., Tayel, A.A., Moussa, S.H., Arru, L., 2021. Green biosynthesized selenium nanoparticles by cinnamon extract and their antimicrobial activity and application as edible coatings with nano-chitosan. *J. Food Qual.* 2021, 1–10.
- Al-saggaf, M.S., 2021. Formulation of insect chitosan stabilized silver nanoparticles with propolis extract as potent antimicrobial and wound healing composites. *Int. J. Polym. Sci.* 2021, 1–9.
- Ameen, F., Al-Maary, K.S., Almansob, A., AlNadhari, S., 2022. Antioxidant, antibacterial and anticancer efficacy of *Alternaria chlamydospora*-mediated gold nanoparticles. *Appl. Nanosci.* <https://doi.org/10.1007/s13204-021-02047-4>.
- Anand, T., Anbukkarasi, M., Thomas, P.A., Geraldine, P., 2021. A comparison between plain eugenol and eugenol-loaded chitosan nanoparticles for prevention of in vitro selenite-induced cataractogenesis. *J. Drug. Deliv. Sci. Technol.* 65., <https://doi.org/10.1016/j.jddst.2021.102696>.
- Argüelles-Monal, W.M., Lizardi-Mendoza, J., Fernández-Quiroz, D., Recillas-Mota, M.T., Montiel-Herrera, M., 2018. Chitosan derivatives: Introducing new functionalities with a controlled molecular architecture for innovative materials. *Polymers* 10 (3), 342. <https://doi.org/10.3390/polym10030342>.
- Avadi, M.R., Sadeghi, A.M.M., Mohammadpour, N., Abedin, S., Atyabi, F., Dinarvand, R., Rafiee-Tehrani, M., 2010. Preparation and characterization of insulin nanoparticles using chitosan and Arabic gum with ionic gelation method. *Nanomed.: Nanotechnol. Biol. Med.* 6, 58–63. <https://doi.org/10.1016/j.nano.2009.04.007>.
- Begum, I., Ameen, F., Soomro, Z., Shamim, S., AlNadhari, S., Almansob, A., Al-Sabri, A., Arif, A., 2021. Facile fabrication of malonic acid capped silver nanoparticles and their antibacterial activity. *J. King Saud Univ. Sci.* 33, (1). <https://doi.org/10.1016/j.jksus.2020.101231>.
- Begum, I., Shamim, S., Ameen, F., Hussain, Z., Bhat, S.A., Qadri, T., Hussain, M., 2022. A Combinatorial approach towards antibacterial and antioxidant activity using tartaric acid capped silver nanoparticles. *Processes* 10 (4), 716. <https://doi.org/10.3390/pr10040716>.

- Bonilla, J., Poloni, T., Lourenço, R.V., Sobral, P.J., 2018. Antioxidant potential of eugenol and ginger essential oils with gelatin/chitosan films. *Food Biosci.* 23, 107–114. <https://doi.org/10.1016/j.fbio.2018.03.007>.
- Das, S., Singh, V.K., Dwivedy, A.K., Chaudhari, A.K., Deepika, Dubey, N.K., 2021. Eugenol loaded chitosan nanoemulsion for food protection and inhibition of Aflatoxin B1 synthesizing genes based on molecular docking. *Carbohydr. Polym.* 255, 117339.
- Espinosa-Andrews, H., Sandoval-Castilla, O., Vazquez-Torres, H., Vernon-Carter, E.J., Lobato-Calleros, C., 2010. Determination of the gum Arabic–chitosan interactions by Fourier Transform Infrared Spectroscopy and characterization of the microstructure and rheological features of their coacervates. *Carbohydr. Polym.* 79, 541–546. <https://doi.org/10.1016/j.carbpol.2009.08.040>.
- Hahn, T., Roth, A., Ji, R., Schmitt, E., Zibek, S., 2020. Chitosan production with larval exoskeletons derived from the insect protein production. *J. Biotechnol.* 310, 62–67. <https://doi.org/10.1016/j.jbiotec.2019.12.015>.
- Hosnedlova, B., Kepinska, M., Skalickova, S., Fernandez, C., Ruttikay-Nedecky, B., Malevu, T.D., Sochor, J., Baron, M., Melcova, M., Zidkova, J., Kizek, R., 2017. A summary of new findings on the biological effects of selenium in selected animal species—a critical review. *Int. J. Mol. Sci.* 18 (10), 2209. <https://doi.org/10.3390/ijms18102209>.
- Ke, C.L., Deng, F.S., Chuang, C.Y., Lin, C.H., 2021. Antimicrobial actions and applications of chitosan. *Polymers.* 13 (6), 904. <https://doi.org/10.3390/polym13060904>.
- Kolahalam, L.A., Viswanath, I.K., Diwakar, B.S., Govindh, B., Reddy, V., Murthy, Y.L.N., 2019. Review on nanomaterials: Synthesis and applications. *Mater. Today: Proc.* 18, 2182–2190. <https://doi.org/10.1016/j.matpr.2019.07.371>.
- Kou, S., Peters, L., Mucalo, M., 2021. Chitosan: A review of sources and preparation methods. *Int. J. Biol. Macromol.* 169, 85–94. <https://doi.org/10.1016/j.ijbiomac.2020.12.005>.
- Kumar, A., Prasad, K.S., 2021. Role of nano-selenium in health and environment. *J. Biotechnol.* 325, 152–163. <https://doi.org/10.1016/j.jbiotec.2020.11.004>.
- Luo, Q., Wang, Y., Han, Q., Ji, L., Zhang, H., Fei, Z., Wang, Y., 2019. Comparison of the physicochemical, rheological, and morphologic properties of chitosan from four insects. *Carbohydr. Polym.* 209, 266–275. <https://doi.org/10.1016/j.carbpol.2019.01.030>.
- Marchese, A., Barbieri, R., Coppo, E., Orhan, I.E., Daglia, M., Nabavi, S.F., Izadi, M., Abdollahi, M., Nabavi, S.M., Ajami, M., 2017. Antimicrobial activity of eugenol and essential oils containing eugenol: A mechanistic viewpoint. *Crit. Rev. Microbiol.* 43 (6), 668–689. <https://doi.org/10.1080/1040841X.2017.1295225>.
- Marei, N., Elwahy, A.H., Salah, T.A., El Sherif, Y., El-Samie, E.A., 2019. Enhanced antibacterial activity of Egyptian local insects' chitosan-based nanoparticles loaded with ciprofloxacin-HCl. *Int. J. Biol. Macromol.* 126, 262–272. <https://doi.org/10.1016/j.ijbiomac.2018.12.204>.
- Marei, N.H., El-Samie, E.A., Salah, T., Saad, G.R., Elwahy, A.H., 2016. Isolation and characterization of chitosan from different local insects in Egypt. *Int. J. Biol. Macromol.* 82, 871–877. <https://doi.org/10.1016/j.ijbiomac.2015.10.024>.
- Mertenat, A., Diener, S., Zurbrugg, C., 2019. Black Soldier Fly biowaste treatment – Assessment of global warming potential. *Waste Manage.* 84, 173–181. <https://doi.org/10.1016/j.wasman.2018.11.040>.
- Moussa, S.H., Tayel, A.A., Al-Turki, A.I., 2013. Evaluation of fungal chitosan as a biocontrol and antibacterial agent using fluorescence-labeling. *Int. J. Biol. Macromol.* 54, 204–208. <https://doi.org/10.1016/j.ijbiomac.2012.12.029>.
- Oluoch, G., Matiru, V., Mamati, E.G., Nyongesa, M., 2021. Nanoencapsulation of thymol and eugenol with chitosan nanoparticles and the effect against *Ralstonia solanacearum*. *Adv. Microbiol.* 11 (12), 723–739. <https://doi.org/10.4236/aim.2021.1112052>.
- Pandit, C., Roy, A., Ghotekar, S., Khuro, A., Islam, M.N., Emran, T.B., Lam, S.E., Khandaker, M.U., Bradley, D.A., 2022. Biological agents for synthesis of nanoparticles and their applications. *J. King Saud Univ. Sci.* 34, (3). <https://doi.org/10.1016/j.jksus.2022.101869>.
- Pant, A., Negi, J.S., 2018. Novel controlled ionic gelation strategy for chitosan nanoparticles preparation using TPP-β-CD inclusion complex. *Eur. J. Pharm. Sci.* 112, 180–185. <https://doi.org/10.1016/j.ejps.2017.11.020>.
- Rajabi, H., Jafari, S.M., Rajabzadeh, G., Sarfarazi, M., Sedaghati, S., 2019. Chitosan-gum Arabic complex nanocarriers for encapsulation of saffron bioactive components. *Colloids Surf. A Physicochem. Eng.* 578, <https://doi.org/10.1016/j.colsurfa.2019.123644>.
- Shao, Y., Wu, C., Wu, T., Li, Y., Chen, S., Yuan, C., Hu, Y., 2018. Eugenol-chitosan nanoemulsions by ultrasound-mediated emulsification: formulation, characterization and antimicrobial activity. *Carbohydr. Polym.* 193, 144–152. <https://doi.org/10.1016/j.carbpol.2018.03.101>.
- Siddiqui, S., Alrumman, S.A., 2021. Influence of nanoparticles on food: An analytical assessment. *J. King Saud Univ. Sci.* 33, (6). <https://doi.org/10.1016/j.jksus.2021.101530>.
- Subramaniyan, S.B., Singaravelu, D.K., Ameen, F., Islam, M.A., Veerappan, A., 2022. Phytolectin-cationic lipid complex revive ciprofloxacin efficacy against multi-drug resistant uropathogenic *Escherichia coli*. *Colloids Surf. A Physicochem. Eng. Asp.* 647, <https://doi.org/10.1016/j.colsurfa.2022.128970>.
- Tan, C., Xie, J., Zhang, X., Cai, J., Xia, S., 2016. Polysaccharide-based nanoparticles by chitosan and gum Arabic polyelectrolyte complexation as carriers for curcumin. *Food Hydrocoll.* 57, 236–245. <https://doi.org/10.1016/j.foodhyd.2016.01.021>.
- Tayel, A.A., El-Tras, W.F., Moussa, S.H., El-Sabbagh, S.M., 2012. Surface decontamination and quality enhancement in meat steaks using plant extracts as natural biopreservatives. *Foodborne Pathog. Dis.* 9, 755–761. <https://doi.org/10.1089/fpd.2012.1203>.
- Tayel, A.A., Moussa, S., Opwis, K., Knittel, D., Schollmeyer, E., Nickisch-Hartfiel, A., 2010. Inhibition of microbial pathogens by fungal chitosan. *Int. J. Biol. Macromol.* 47, 10–14. <https://doi.org/10.1016/j.ijbiomac.2010.04.005>.
- Tayel, A.A., Elzahy, A.F., Moussa, S.H., Al-Saggaf, M.S., Diab, A.M., Puértolas, E., 2020. Biopreservation of shrimps using composed edible coatings from chitosan nanoparticles and cloves extract. *J. Food Qual.* 2020, 1–10.
- Wang, Q., Zhang, L., Ding, W., 2020. Eugenol nanocapsules embedded with gelatin-chitosan for chilled pork preservation. *Int. J. Biol. Macromol.* 158, 837–844. <https://doi.org/10.1016/j.ijbiomac.2020.04.182>.
- Woranuch, S., Yoksan, R., 2013. Eugenol-loaded chitosan nanoparticles: I. Thermal stability improvement of eugenol through encapsulation. *Carbohydr. Polym.* 96 (2), 578–585. <https://doi.org/10.1016/j.carbpol.2012.08.117>.
- Yassin, M.T., Al-Askar, A.A., Mostafa, A.A.F., El-Sheikh, M.A., 2020. Bioactivity of *Syzygium aromaticum* (L.) Merr. & LM Perry extracts as potential antimicrobial and anticancer agents. *J. King Saud Univ. Sci.* 32 (8), 3273–3278. <https://doi.org/10.1016/j.jksus.2020.09.009>.
- Zaynab, M., Al-Yahyai, R., Ameen, A., Sharif, Y., Ali, L., Fatima, M., Khan, K.A., Li, S., 2022. Health and environmental effects of heavy metals. *J. King Saud Univ. Sci.* 34, (1). <https://doi.org/10.1016/j.jksus.2021.101653>.
- Zhang, J.S., Gao, X.Y., Zhang, L.D., Bao, Y.P., 2001. Biological effects of a nano red elemental selenium. *Biofactors* 15 (1), 27–38. <https://doi.org/10.1002/biof.5520150103>.